Electronic Supplementary Material (ESI) for Nanoscale.

Supporting Information

Giant intrinsic photovoltaic effect in atomically thin ReS_2

Jing Wang, [a] *Nannan Han,* *[b] *Zhihua Lin,* [b] *Siqi Hu,* [a] *Ruijuan Tian,* [a] *Mingwen Zhang,* [a] *Yu Zhang,* [a] *Jianlin Zhao* [a] *and Xuetao Gan* *[a]

a. Key Laboratory of Light Field Manipulation and Information Acquisition, Ministry of Industry and Information Technology, and Shaanxi Key Laboratory of Optical Information Technology, School of Physical Science and Technology, Northwestern Polytechnical University, Xi'an, 710129 China

b. Frontiers Science Center for Flexible Electronics, Institute of Flexible Electronics, Northwestern Polytechnical University, Xi'an 710072, China

*E-mail: xuetaogan@nwpu.edu.cn

*E-mail: iamnnhan@nwpu.edu.cn

1. Second harmonic generation (SHG) in tetralayer ReS_2

Fig. S1a shows the optical microscope image of the fabricated tetralayer ReS_2 photovoltaic (PV) device. The SHG characteristic of the individual tetralayer ReS_2 (marked by the red star in Fig. S1a) was evaluated under a home-built vertical microscope setup with the reflection geometry. A fiber-based picosecond pulsed laser was employed as the fundamental pump radiation, which has a central wavelength around 1550 nm, a repetition rate of 18.5 MHz and a pulse width of 8.8 ps. The pulsed laser was focused by a 50× objective lens with a numerical aperture of 0.75 into a spot size about 2 μm on the sample. The SHG response scattered from the sample was collected by the same objective lens, which was then examined by a spectrometer mounted with a cooled silicon CCD camera. The collected spectra from tetralayer ReS_2 at the range around the half of the pump wavelength are plotted in Fig. S1b. The strong SHG signal indicates that the tetralayer ReS_2 is non-centrosymmetry.[1-3]

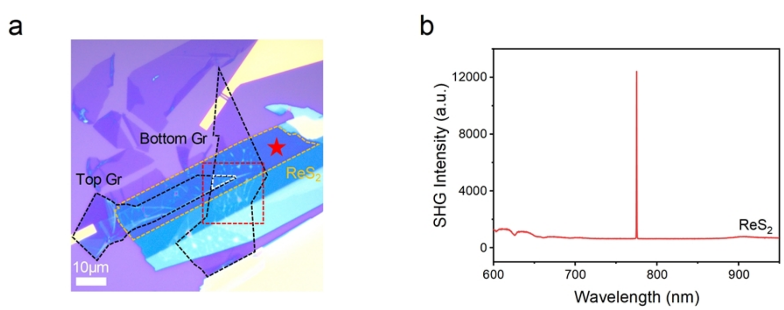

Fig. S1 (a) Optical microscope image of the fabricated tetralayer ReS_2 PV device. (b) SHG spectra measured from the individual tetralayer ReS_2 marked by the red star in Fig. S1a.

2. Atomic force microscopy (AFM) of the tetralayer ReS_2

The layer number of ReS_2 in Fig. 1b is also confirmed by the atomic force microscopy (AFM), as shown in Fig. S2. The inset shows the height data measured along the white dotted line with a value of ~3.309 nm, corresponding to the thickness of tetralayer.

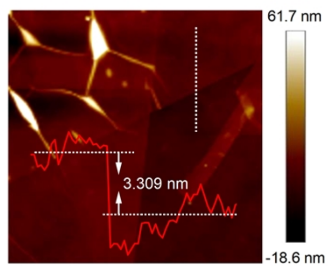

Fig. S2 AFM image of the tetralayer ReS_2.

3. Electrical characteristics in tetralayer ReS_2

The electrical characteristics of the device in Fig. 1b under different gate voltages without laser illumination are shown in Fig. S3. By applying source-drain voltages (V_{DS}) from -1 to 1 mV, the obtained source-drain currents (I_{DS}) under different gate voltages (V_G) are shown in Fig. S3a. Under different V_G, the I_{DS} - V_{DS} curves all show linear and symmetric cross the origin. We calculated the rectification ratios under different V_G, as shown in Fig. S3b. The rectification ratios under different V_G are all almost equal to one. The results above indicate that even though there are different electrostatic dopings of the bottom graphene under different V_G, the top and bottom graphene electrodes are symmetric and have good Ohmic contact with ReS_2.

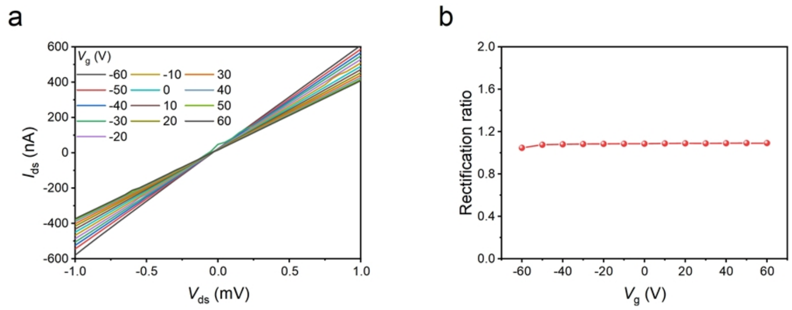

Fig. S3 (a) I_{DS} - V_{DS} curves of the tetralayer ReS_2 based PV device as measured under different V_G in dark conditions. (b) Rectification ratios extracted from the results in (a).

4. Absorption characteristics of tetralayer ReS_2

We perform differential reflection measurements to characterize the absorption properties of the tetralayer ReS_2 on the SiO_2 substrate. The result is shown in Fig. S4. Here, the differential reflection is defined as $\Delta R/R_0 = (R-R_0)/R_0$, where R and R_0 are the reflectances of the ReS_2 sample and the SiO_2 substrate, respectively. Because of the interfering reflection of the 300-nm-thick SiO_2 substrate, the optical absorption of the tetralayer ReS_2 is enhanced around the wavelength of 530 nm. Therefore, the PV effect of the tetralayer ReS_2 is strongest at around 530 nm.

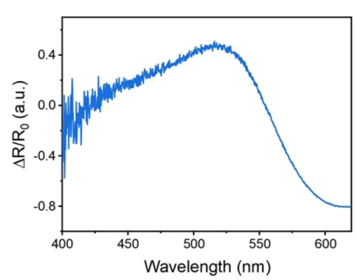

Fig. S4 Differential reflection spectrum of the tetralayer ReS_2.

5. Dynamic response in the tetralayer ReS_2 device

The response time can be obtained by analyzing the rise time (τ_r) and fall time (τ_f) of rising and falling edges, estimated between 10% and 90% of the maximum I_{sc}. Therefore, the τ_r/τ_f was calculated to be 146/125 μs with the laser illumination modulated at 500 Hz, as shown in Fig. S5a. Fig. S5b shows the dynamic response of the photocurrent in tetralayer ReS_2 device illuminated with the laser modulated at 4 kHz, and the τ_r/τ_f was calculated to be 70.2/79.4 μs, as shown in Fig. S5c.

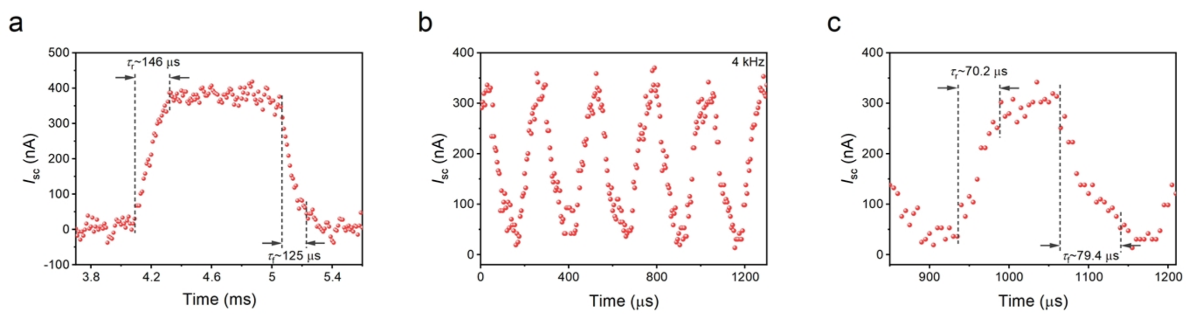

Fig. S5 (a) Rising and falling edges for estimating the rise time (τ_r) and the fall time (τ_f) at the laser on/off modulation frequency of 500 Hz. (b) Dynamic response of the photocurrent at the laser on/off modulation frequency of 4 kHz. (c) Rising and falling edges for estimating the rise time (τ_r) and the fall time (τ_f) at the laser on/off modulation frequency of 4 kHz.

6. PV effect in six-layer ReS_2

The optical microscope image of the six-layer ReS_2 PV device is shown in Fig. S6a. The SHG spectra of the individual six-layer ReS_2 marked by the red star in Fig. S6a is shown in Fig. S6b. The strong SHG signal indicates that the six-layer ReS_2 is non-centrosymmetry.[1-3] Fig. S6c shows the Raman spectroscopy of ReS_2 in Fig. S6a. The characteristic peak of 29.10 cm^{-1} in the ultralow-frequency spectrum indicates that the layer number of ReS_2 in Fig. S6a is six. In the high-frequency spectrum, the characteristic peaks of 160.86, 212.47 and 235.85 cm^{-1} are consistent with the results of ReS_2 in the previous literature.[4]

Without illumination, the obtained source-drain currents (I_{DS}) with the source-drain voltages (V_{DS}) between -1 and 1 mV were shown in the black curve in Fig. S6d. The linear I_{DS} - V_{DS} curve crosses the origin indicating the good Ohmic contacts between the multilayer graphene electrodes and the ReS_2 channel. When illuminated the sandwich structure region with the laser wavelength of 532 nm, the linear I_{DS} - V_{DS} curve was shifted upwards significantly, indicating a non-negligible PV behavior, as shown in the red curve in Fig. S6d.

The laser polarization dependence of I_{sc} in six-layer ReS_2 is shown in Fig. S6e. The result is anisotropic with no sign change when rotating the polarization direction, which is attributed to the in-plane non-centrosymmetry of six-layer ReS_2. Fig. S6f shows the laser power dependence of I_{sc} in six-layer ReS_2. Same as that in tetralayer ReS_2, the laser power dependence of I_{sc} in the six-layer ReS_2 still shows linear feature even under high power intensity. This unique characteristic indicates the depolarization field should be the dominant mechanism of the PV effect generation in atomically thin ReS_2.[5]

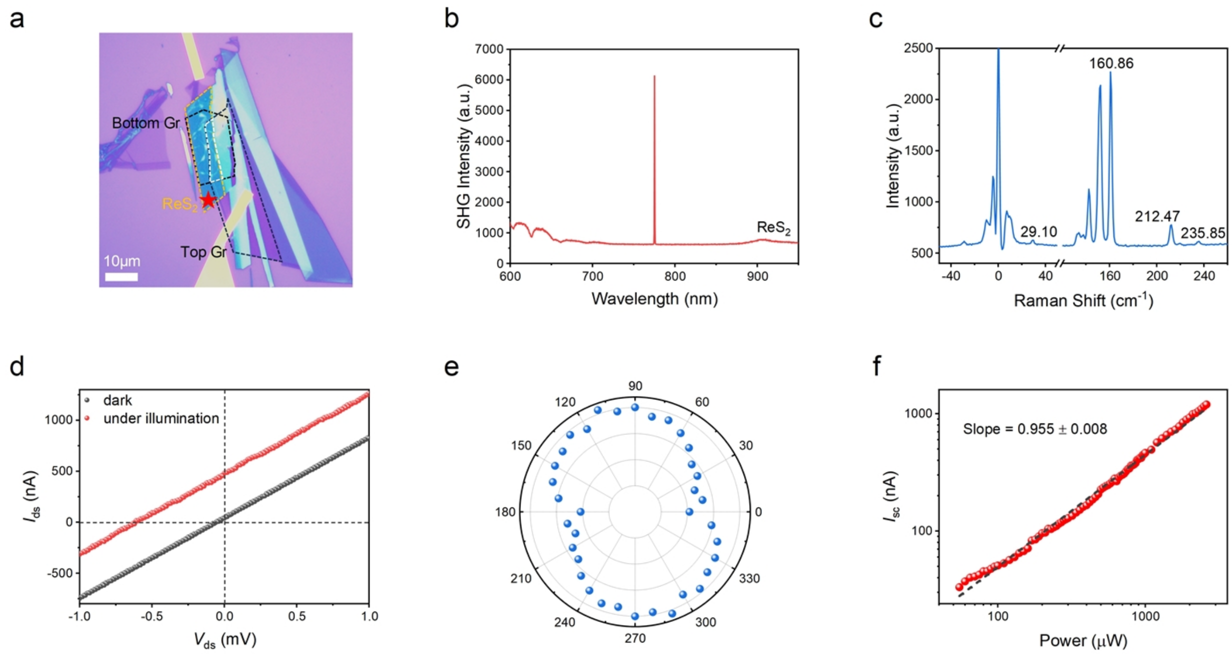

Fig. S6 (a) Optical microscope image of the six-layer ReS_2 PV device. (b) SHG spectra measured from the individual six-layer ReS_2 marked by the red star in Fig. S6a. (c) Raman spectrum of the six-layer ReS_2 in Fig. S6a. (d) I_{DS} - V_{DS} curves of the six-layer ReS_2 PV device as measured in dark (black) and illuminated (λ = 532 nm, red) conditions. (e) Polar plot of I_{sc} with respect to the polarization of the pump laser measured from the six-layer ReS_2 PV device. (f) Laser power dependence of I_{sc} in six-layer ReS_2.

7. PV effect in trilayer ReS_2

The optical microscope image of the trilayer ReS_2 PV device is shown in Fig. S7a. The SHG spectra of the individual trilayer ReS_2 marked by the red star in Fig. S7a is shown in Fig. S7b. The nearly no measurable SHG signal indicates that the trilayer ReS_2 is centrosymmetry.[1-3] Fig. S7c shows the Raman spectroscopy of ReS_2 in Fig. S7a. The characteristic peak of 21.31 cm^{-1} in the ultralow-frequency spectrum indicates that the layer number of ReS2 in Fig. S7a is three. In the high-frequency spectrum, the characteristic peaks of 160.86, 211.71 and 236.60 cm^{-1} are consistent with the results of ReS_2 in the previous literature.[4]

Without illumination, the obtained source-drain currents (I_{DS}) with the source-drain voltages (V_{DS}) between -1 and 1 mV were shown in the black curve in Fig. S7d. The linear I_{DS} - V_{DS} curve crosses the origin indicates the good Ohmic contacts between the multilayer graphene electrodes and the ReS_2 channel. When illuminated the sandwich structure region with the laser wavelength of 532 nm, the linear I_{DS} - V_{DS} curve keep almost unchanged, indicating no obvious PV behavior, as shown in the red curve in Fig. S7d. These results illustrate the centrosymmetry-breaking is essential for the PV effect generation in atomically thin ReS_2.

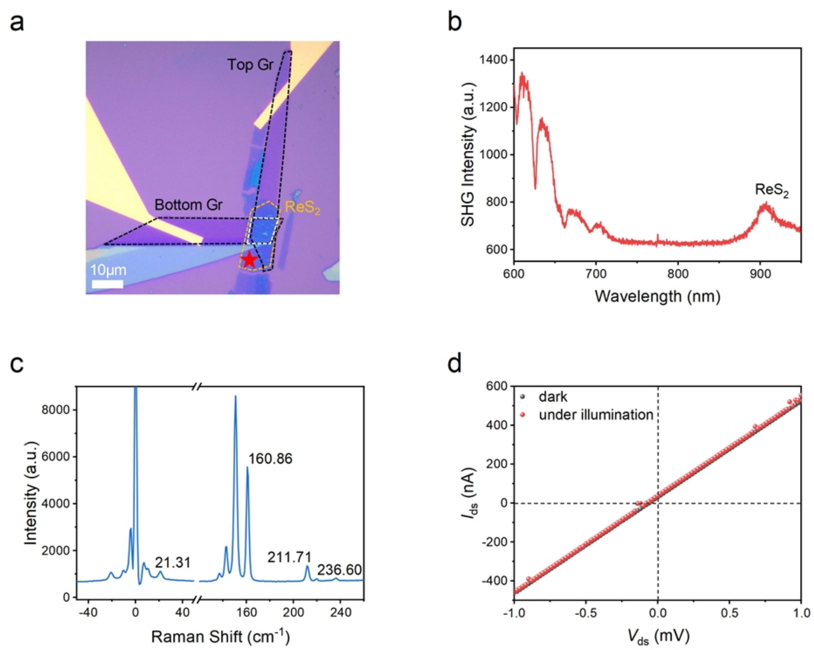

Fig. S7 (a) Optical microscope image of the trilayer ReS_2 PV device. (b) SHG spectra measured from the individual trilayer ReS_2 marked by the red star in Fig. S7a. (c) Raman spectrum of the trilayer ReS_2 in Fig. S7a. (d) I_{DS} - V_{DS} curves of the trilayer ReS_2 PV device as measured in dark (black) and illuminated (λ = 532 nm, red) conditions.

8. Computational methods

All calculations were performed by VASP code according to the density functional theory (DFT)[6,7] with the PBE functional[8] and the projected augmented wave potential method.[9] During the calculation, the unit cell of tetralayer ReS_2 was used and the thickness of vacuum was larger than 15 Å. The energy cutoff for plane-wave basis was set to 500 eV. The atomic structures were relaxed until the forces less than 0.001 eV/Å and the energy less than 10^{-5} eV. The reciprocal space is sampled by a grid of 7×7×1 in the Brillouin zone. The polarization intensity was obtained through Berry-phase calculation.[10]

REFERENCES

(1) Y. Song, S. Hu, M. L. Lin, X. Gan, P. H. Tan and J. Zhao, *ACS Photonics*, 2018, **5**, 3485–3491.

(2) J. Wang, N. Han, Z.-D. Luo, M. Zhang, X. Chen, Y. Liu, Y. Hao, J. Zhao and X. Gan, *ACS Nano*, 2022, **16**, 6404–6413.

(3) J. Wang, M. Zhang, N. Han, Z. Luo, X. Chen, Y. Liu, J. Zhao and X. Gan, *Adv. Opt. Mater.*, 2023, **11**, 2202495.

(4) X. F. Qiao, J. Bin Wu, L. Zhou, J. Qiao, W. Shi, T. Chen, X. Zhang, J. Zhang, W. Ji and P. H. Tan, *Nanoscale*, 2016, **8**, 8324–8332.

(5) D. Yang, J. Wu, B. T. Zhou, J. Liang, T. Ideue, T. Siu, K. M. Awan, K. Watanabe, T. Taniguchi, Y. Iwasa, M. Franz and Z. Ye, *Nat. Photonics*, 2022, **16**, 469–474.

(6) G. Kresse and J. Furthmüller, *Comput. Mater. Sci.*, 1996, **6**, 15–50.

(7) G. Kresse and J. Furthmüller, *Phys. Rev. B - Condens. Matter Mater. Phys.*, 1996, **54**, 11169–11186.

(8) J. P. Perdew, K. Burke and M. Ernzerhof, *Phys. Rev. Lett.*, 1996, **77**, 3865–3868.

(9) P. E. Blöchl, *Phys. Rev. B*, 1994, **50**, 17953–17979.

(10) R. Fei, W. Kang and L. Yang, *Phys. Rev. Lett.*, 2016, **117**, 097601.